

# New cluster approach on properties of $^{8-11}\text{Be}$ isotopes with isospin-dependent spin-orbit potential

Mengjiao Lyu,<sup>1,2,\*</sup> Zhongzhou Ren,<sup>1,3,†</sup> Hisashi Horiuchi,<sup>2,4,‡</sup> Bo Zhou,<sup>5</sup> Yasuro Funaki,<sup>6</sup>  
Gerd Röpke,<sup>7</sup> Peter Schuck,<sup>8,9</sup> Akihiro Tohsaki,<sup>2</sup> Chang Xu,<sup>1</sup> and Taiichi Yamada<sup>10</sup>

<sup>1</sup>*Department of Physics, Nanjing University, Nanjing 210093, China*

<sup>2</sup>*Research Center for Nuclear Physics (RCNP),*

*Osaka University, Osaka 567-0047, Japan*

<sup>3</sup>*School of Physics Science and Engineering,*

*Tongji University, Shanghai 200092, China*

<sup>4</sup>*International Institute for Advanced Studies, Kizugawa 619-0225, Japan*

<sup>5</sup>*Faculty of Science, Hokkaido University, Sapporo 060-0810, Japan*

<sup>6</sup>*School of Physics and Nuclear Energy Engineering,*

*Beihang University, Beijing 100191, China*

<sup>7</sup>*Institut für Physik, Universität Rostock, D-18051 Rostock, Germany*

<sup>8</sup>*Institut de Physique Nucléaire, Université Paris-Sud,*

*IN2P3-CNRS, UMR 8608, F-91406, Orsay, France*

<sup>9</sup>*Laboratoire de Physique et Modélisation des Milieux Condensés,*

*CNRS-UMR 5493, F-38042 Grenoble Cedex 9, France*

<sup>10</sup>*Laboratory of Physics, Kanto Gakuin University, Yokohama 236-8501, Japan*

(Dated: December 30, 2021)

## Abstract

The nonlocalized clustering approach is generalized to  $^8\text{--}^{11}\text{Be}$  isotopes with isospin dependent spin-orbit potential. A new form of the Tohsaki-Horiuchi-Schuck-Röpke (THSR) wave function is introduced to provide a correct description for the  $\sigma$ -binding neutron in  $^{11}\text{Be}$ . Systematic calculations for  $^8\text{--}^{11}\text{Be}$  isotopes are performed and results fit well with experimental values. The low energy spectrum of  $^{11}\text{Be}$  is also obtained, especially the correct spin-parity  $1/2^+$  is reproduced for the intruder ground state. The exotic neutron halo structure of  $^{11}\text{Be}$  is studied by calculations of root-mean-square radii and density distribution. We obtain a large spatial distribution for the last valence neutron of  $^{11}\text{Be}$ , which fits the phenomenological extracted value from experimental data. The spectroscopic factor is also calculated and discussed for the  $1/2^+$  ground state of  $^{11}\text{Be}$ .

---

\* mengjiao\_lyu@hotmail.com

† zren@nju.edu.cn

‡ horiuchi@rcnp.osaka-u.ac.jp

The studies of various spin-orbit interactions illuminate important effects and mechanisms in different fields of physics. Especially, a large spin-orbit interaction is introduced in the development of the nuclear shell model to reproduce the magic numbers such as 28, 50, 82, and 126 for the  $\beta$ -stable nuclei [1]. In recent investigations, the spin-orbit coupling induces anomalous Hall effects in tunnel junction or in nonmagnetic metals [2, 3]. The spin-orbit coupling also plays a key role in various models for the understanding of topological insulators [4, 5]. Other prominent spin-orbit coupling effects include the fine structure in atomic spectra and magnetocrystalline anisotropy for materials [6, 7].

For neutron-rich nuclei which are away from the  $\beta$ -stable line, spin-orbit couplings provide large contributions for the binding of the valence neutrons [8, 9]. Experimentally, the neutron-rich nucleus  $^{11}\text{Be}$  is famous for its exotic properties including neutron halo structure and abnormal positive ground state parity [10–15]. The key role of large spin-orbit interaction has been discussed in some pioneer works including studies with antisymmetrized molecular dynamics and shell model calculations [9, 14, 16, 17]. The dominance of clustering effects in many Be isotopes including  $^{11}\text{Be}$  are also confirmed in theoretical and experimental studies [18–20]. Thus, a new clustering approach with spin-orbit interaction is essential for a valid description of the structure and dynamics of the Be isotopes.

In recent years, the clustering effects and the halo structures in nuclei have been extensively studied with various approaches [18–36]. Especially, the Tohsaki-Horiuchi-Schuck-Röpke (THSR) wave function with intrinsic cluster degree of freedom is proposed and underlies the new nonlocalized concept for cluster dynamics [18, 22–27]. Then in our previous studies, valence neutrons with spin-orbit interaction are treated in this model, what successfully reproduces the physical properties of  $^{9-10}\text{Be}$  isotopes and illustrates the dynamics of  $\alpha$ -clusters and valence neutrons [19, 20].

In this work, a new improved form of the THSR wave function is proposed for the nucleus  $^{11}\text{Be}$ . With a new introduced isospin-dependent spin-orbit interaction strength, we perform the first systematic calculations for the  $^{8-11}\text{Be}$  isotopes with the THSR wave function. The calculated physical properties agree well with experimental results. Exotic properties of  $^{11}\text{Be}$  such as the inversion of two lowest states and the large halo structure in the ground state are also well described.

The THSR wave function of  $^{11}\text{Be}$  nucleus is formulated in the form of creation operators,

as

$$|\Phi(\text{Be})\rangle = (C_\alpha^\dagger)^2 c_n^\dagger(9) c_n^\dagger(10) c_n^\dagger(11) |\text{vac}\rangle, \quad (1)$$

where  $C_\alpha^\dagger$  and  $c_n^\dagger$  are creation operators of  $\alpha$ -clusters and valence neutrons, respectively. For the two  $\alpha$ -clusters in the  $^8\text{Be}$  core, the  $\alpha$ -creators  $C_\alpha^\dagger$  are written as

$$C_\alpha^\dagger = \int d\mathbf{R} \exp\left(-\frac{R_x^2 + R_y^2}{\beta_{\alpha,xy}^2} - \frac{R_z^2}{\beta_{\alpha,z}^2}\right) \int d\mathbf{r}_1 \cdots d\mathbf{r}_4 \quad (2)$$

$$\times \psi(\mathbf{r}_1 - \mathbf{R}) a_{\sigma_1, \tau_1}^\dagger(\mathbf{r}_1) \cdots \psi(\mathbf{r}_4 - \mathbf{R}) a_{\sigma_4, \tau_4}^\dagger(\mathbf{r}_4),$$

where  $\mathbf{R}$  is the generate coordinate of the  $\alpha$ -cluster and  $a_{\sigma, \tau}^\dagger(\mathbf{r}_i)$  creates the  $i$ -th nucleon with spin  $\sigma$  and isospin  $\tau$  at position  $\mathbf{r}_i$ .  $\psi(\mathbf{r}) = (\pi b^2)^{-3/4} \exp(-r^2/2b^2)$  is the single nucleon wave function. Parameter  $b$  is chosen to be  $b = 1.35$  in this Gaussian function to optimize the binding energy of  $\alpha$ -cluster.  $\beta_{\alpha,xy}$  and  $\beta_{\alpha,z}$  are deformation parameters for the nonlocalized motion of two  $\alpha$ -clusters.

Generally, the neutron creators  $c_n^\dagger$  for the  $i$ -th valence neutron can be written in the following form as

$$c_n^\dagger(i) = \int d\mathbf{R}_i \exp\left(-\frac{R_{i,x}^2 + R_{i,y}^2}{\beta_{i,xy}^2} - \frac{R_{i,z}^2}{\beta_{i,z}^2}\right) \int d\mathbf{r}_i \quad (3)$$

$$\times (\pi b^2)^{-3/4} f(\mathbf{R}_i, \dots) e^{-(\mathbf{r}_i - \mathbf{R}_i)^2/(2b^2)} a_\sigma^\dagger(\mathbf{r}_i).$$

Here  $\sigma$  is the spin of the valence neutron and  $a_\sigma^\dagger(\mathbf{r}_i)$  creates the  $i$ -th neutron with spin  $\sigma$  at position  $\mathbf{r}_i$ .  $\beta_{i,xy}$  and  $\beta_{i,z}$  are also nonlocalization parameters for the  $i$ -th valence neutron in a deformed orbit. This expression has a similar form as the  $\alpha$ -cluster creators in Eq. 2 except for the introduction of extra factor  $f(\mathbf{R}_i, \dots)$ .

For creators  $c_n^\dagger(9)$  and  $c_n^\dagger(10)$  of the first two valence neutrons in  $^{11}\text{Be}$ , we adopt the extra factor as  $f(\mathbf{R}_{9,10}, \dots) = e^{im\phi_{\mathbf{R}_{9,10}}}$ , where parameter  $m = 1$  with spin  $\sigma = |\uparrow\rangle$  and  $m = -1$  with spin  $\sigma = |\downarrow\rangle$ . These two extra factors ensure negative parity for the each single neutron wave function and provide good description for their  $\pi$ -binding structure as we discussed in our previous works.

For the last valence neutron of the  $^{11}\text{Be}$  nucleus, we adopt different creators for the  $1/2^+$  and  $1/2^-$  rotational bands. For the positive parity states, we propose a new creation

operator as

$$\begin{aligned}
c_n^\dagger(11) = & \int d\mathbf{R}_{11} \exp \left( -\frac{R_{11,x}^2 + R_{11,y}^2}{\beta_{11,xy}^2} - \frac{R_{11,z}^2}{\beta_{11,z}^2} \right) \\
& \times \left[ e^{-\frac{R_{11,x}^2 + R_{11,y}^2}{\gamma a^2} - \frac{R_{11,z}^2}{a^2}} - e^{-(\mathbf{R}_1 - \mathbf{R}_2)^2 / (2a)^2} \right] \\
& \times \int d\mathbf{r}_{11} (\pi b^2)^{-3/4} e^{-(\mathbf{r}_{11} - \mathbf{R}_{11})^2 / (2b^2)} a_n^\dagger(\mathbf{r}_{11}).
\end{aligned} \tag{4}$$

In this neutron creator, a new extra factor

$$\begin{aligned}
f(\mathbf{R}_{11}, \dots) = & \exp \left( -\frac{R_{11,x}^2 + R_{11,y}^2}{\gamma a^2} - \frac{R_{11,z}^2}{a^2} \right) \\
& - \exp \left( -(\mathbf{R}_1 - \mathbf{R}_2)^2 / (2a)^2 \right)
\end{aligned} \tag{5}$$

is introduced for a correct description of the nodal structure of the  $\sigma$ -orbit wave function for the last valence neutron. The generator coordinates  $\mathbf{R}_1$  and  $\mathbf{R}_2$  of two  $\alpha$ -clusters are also included in this creator to describe the correlation between the valence neutron and  $\alpha$ -clusters. We provide the analytical expression of the single nucleon wave function  $\phi_n(\mathbf{r}) = \langle \mathbf{r} | c_n^\dagger(i=11) | \text{vac} \rangle$  for the last valence neutron in the  $1/2^+$  ground state of  $^{11}\text{Be}$ , as

$$\begin{aligned}
\phi_n(\mathbf{r}) = & \prod_{\xi=x,y,z} \left\{ \sqrt{\frac{1}{b^2} + \frac{2}{B_\xi^2}} \exp \left( -\frac{r_\xi^2}{2b^2 + B_\xi^2} \right) \right. \\
& \left. - \sqrt{\frac{1}{b^2} + \frac{2}{\beta_\xi^2}} \exp \left( -\frac{(\mathbf{R}_1 - \mathbf{R}_2)^2}{(2a)^2} - \frac{r_\xi^2}{2b^2 + \beta_\xi^2} \right) \right\}.
\end{aligned} \tag{6}$$

Here, the subscript  $\xi$  stands for each of the  $x, y$  and  $z$  coordinates.  $1/B_\xi^2 = 1/\beta_\xi^2 + 1/(\gamma a)^2$  for  $x$  and  $y$  coordinates and  $1/B_\xi^2 = 1/\beta_\xi^2 + 1/a^2$  for the  $z$  coordinate. In Fig. 1, we show the  $y = 0$  cross section for this single neutron wave function. An ellipsoidal nodal surface is clearly demonstrated in this figure with green color. Along the  $z$ -axis, the nodes with green color are physically the most likely locations for  $\alpha$ -clusters.

For the  $1/2^-$  rotational band of  $^{11}\text{Be}$  with negative parity, we formulate  $c_n^\dagger(11)$  with similar form as  $c_n^\dagger(9)$  and  $c_n^\dagger(10)$  but with antiparallel spin-orbit coupling.

The Hamiltonian of the  $^{11}\text{Be}$  system can be written as

$$H = \sum_{i=1}^{11} T_i - T_{c.m.} + \sum_{i < j}^{11} V_{ij}^N + \sum_{i < j}^{11} V_{ij}^C + \sum_{i < j}^{11} V_{ij}^{ls}, \tag{7}$$

where  $T_{c.m.}$  is the kinetic energy of the center-of-mass motion. Volkov No. 2 is used as the central force of the nucleon-nucleon potential,

$$V_{ij}^N = \{V_1 e^{-\alpha_1 r_{ij}^2} - V_2 e^{-\alpha_2 r_{ij}^2}\} \{W - M \hat{P}_\sigma \hat{P}_\tau + B \hat{P}_\sigma - H \hat{P}_\tau\}, \tag{8}$$

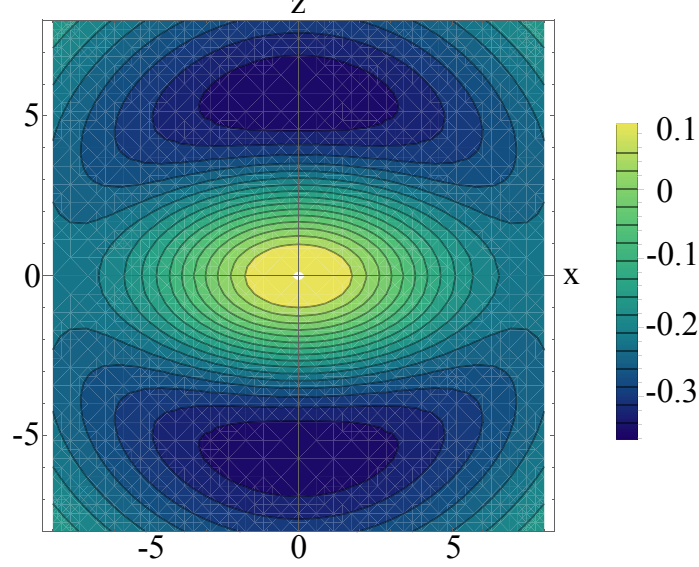


FIG. 1. The  $y = 0$  cross section of the single nucleon wave function  $\phi_n(\mathbf{r})$  for the last valence neutron in the  $1/2^+$  ground state of  $^{11}\text{Be}$ . The yellow color denotes positive values of  $\phi_n(\mathbf{r})$ . The blue color denotes negative values of  $\phi_n(\mathbf{r})$ . The green color denotes values close to zero of  $\phi_n(\mathbf{r})$ . Parameters are chosen as  $b = 1.35$  fm,  $\beta_{11,xy} = \beta_{11,z} = 10$  fm,  $a = 3$  fm,  $\gamma = 2$  and  $|\mathbf{R}_1 - \mathbf{R}_2| = 1.3$  fm.

where  $M = 0.6$ ,  $W = 0.4$  and  $B = H = 0.125$ . Other parameters are  $V_1 = -60.650$  MeV,  $V_2 = 61.140$  MeV,  $\alpha_1 = 0.309$  fm $^{-2}$ , and  $\alpha_2 = 0.980$  fm $^{-2}$ . The G3RS (Gaussian soft core potential with three ranges) term is taken as the two-body type spin-orbit interaction,

$$V_{ij}^{ls} = V_0^{ls} \{e^{-\alpha_1 r_{ij}^2} - e^{-\alpha_2 r_{ij}^2}\} \mathbf{L} \cdot \hat{\mathbf{S}} \hat{P}_{31}, \quad (9)$$

where  $\hat{P}_{31}$  projects the two-body system into triplet odd state. An isospin-dependent spin-orbit interaction strength is adopted in our calculations, as

$$V_0^{ls} = 2400 + 200 \times |N - Z| \quad (\text{MeV}) \quad (10)$$

Other parameters in  $V_{ij}^{ls}$  are  $\alpha_1 = 5.00$  fm $^{-2}$ , and  $\alpha_2 = 2.778$  fm $^{-2}$ .

We perform systematic calculations for the binding energies of  $^{8-11}\text{Be}$  isotopes. The results are listed in Table I and shown in Fig. 2. The binding energies calculated with the THSR wave function are found to be in good agreement with corresponding experimental values. The  $0^+$  ground state of  $^8\text{Be}$ , which is closely below the two  $\alpha$  threshold, is correctly reproduced. The one neutron separation energies  $S_n$  of Be isotopes, as displayed in Fig. 3, also fit corresponding experimental data.

TABLE I. Calculated results of the ground states of Be isotopes. “E (THSR)” denotes results calculated with the THSR wave function. “ $V_{ls}^*$ ” denotes corresponding spin-orbit interaction strength. “E (Exp)” denotes experimental values adopted from Ref. [38]. All units are in MeV.

	E (THSR)	E (Exp) [38]	$V_{ls}^*$
$^{11}\text{Be}(1/2^+)$	-64.6	-65.5	3000
$^{10}\text{Be}(0^+)$	-63.9	-65.0	2800
$^9\text{Be}(3/2^-)$	-56.5	-58.2	2600
$^8\text{Be}(0^+)$	-55.9	-56.5	2400

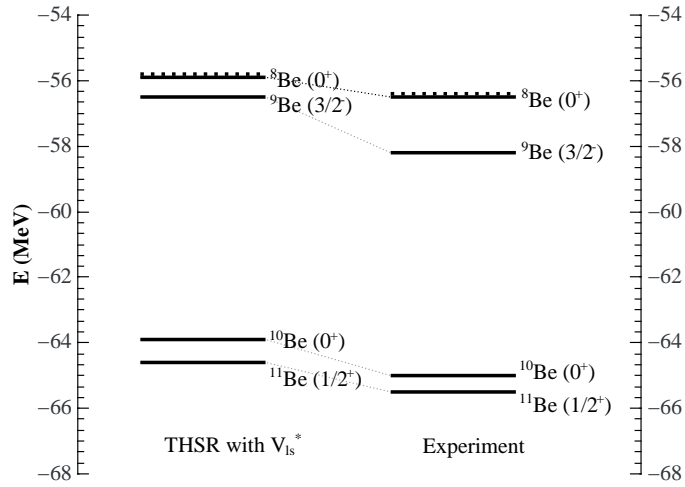


FIG. 2. The ground state energies of  $^8$ - $^{11}\text{Be}$  isotopes. “THSR with  $V_{ls}^*$ ” denotes calculated results with the THSR wave function and the modified spin-orbit interaction strength. “Experiment” denotes the experimental values from Ref. [38]. The dashed lines indicate the corresponding  $\alpha + n + \dots$  threshold.

For the intruder ground state of  $^{11}\text{Be}$ , the exotic positive parity is also correctly reproduced. As shown in Fig. 4, the spin-orbit strength plays a key role for the level order for the lowest  $1/2^+$  and  $1/2^-$  states. It is shown that with the weaker  $V_0^{ls} = 2000$  MeV strength, a negative parity is obtained for the ground state. With the new strength  $V_0^{ls*} = 3000$  MeV, which is 1000 MeV larger, the level order of the  $1/2^+$  and  $1/2^-$  states is inverted. This inversion is due to that the spin-orbit coupling in the  $1/2^+$  ground state is larger than the one in the  $1/2^-$  state, where the last valence neutron has antiparallel spin-orbit cou-

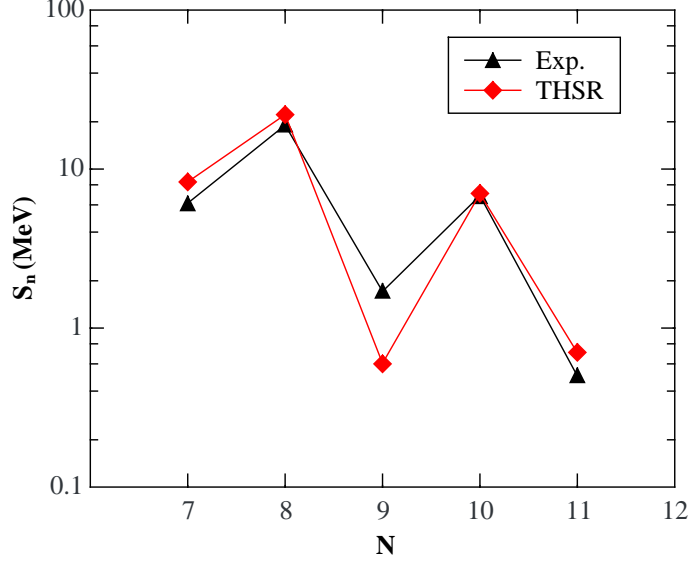


FIG. 3. The one-neutron separation energies  $S_n$  of  ${}^6\text{--}{}^{11}\text{Be}$  isotopes. “THSR” denotes calculated results with the THSR wave function and “Exp” denotes the experimental values from Ref. [38].

pling. We also see great improvement for the low lying rotational band in Fig. 4, which fits the experimental values reasonably well. However, despite the correct ordering the spectrum stays quite a bit too diluted compared with experiment. In the phenomenological particle-vibration coupling (PVC) model of Vinh Mau [40], the spreading of the states is much reduced. This is probably due to the fact that experimental values of BE2 and other transition values are taken as input. Nevertheless, this hints to the fact that an explicit account of some low lying collective states of the  ${}^{10}\text{Be}$  core is needed. In our approach there is no adjustable parameter besides the increased spin-orbit strength but this is also the case in Ref. [40].

The  ${}^{11}\text{Be}$  is also well known for its neutron halo structure. This exotic property is studied with our THSR wave function by calculating the root-mean-square radii for the ground state of  ${}^{11}\text{Be}$ , as listed in Table II. It is found that the neutrons have a much larger RMS radius than the protons in the ground state  ${}^{11}\text{Be}$ . This indicates that the  $1/2^+$  ground state of  ${}^{11}\text{Be}$  has a neutron halo structure, which is consistent with the experimental observations. In our calculations, the large difference between neutron and proton radii comes mainly from the large spread of the last valence neutron occupying the  $\sigma$ -orbit. In fact, a giant RMS radius 8.94 fm is obtained for the last valence neutron, which agrees with the giant value 7.98 fm extracted phenomenologically from experimental data [41].

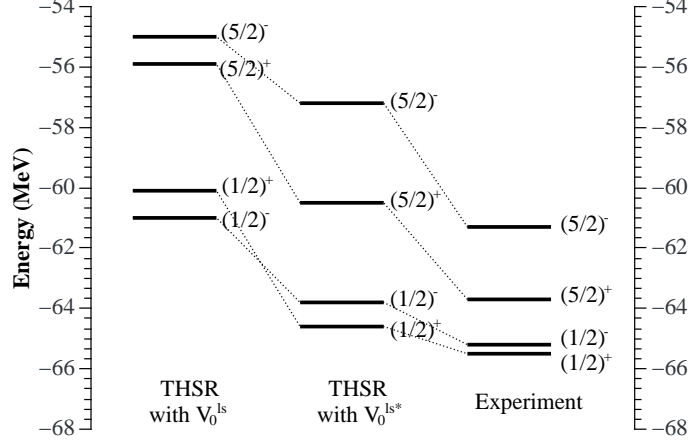


FIG. 4. The energy spectrum for the low lying states of  $^{11}\text{Be}$ . “THSR with  $V_0^{ls}$ ” denotes calculated results with fixed spin-orbit interaction strength  $V_0^{ls} = 2000$  MeV. “THSR with  $V_0^{ls*}$ ” denotes calculated results with the modified spin-orbit interaction strength  $V_0^{ls*} = 3000$  MeV. “Experiment” denotes the experimental values from Ref. [39].

TABLE II. Matter, proton and neutron root-mean-square (RMS) radii of the ground state of  $^{11}\text{Be}$  denoted by  $\langle r_m^2 \rangle^{1/2}$ ,  $\langle r_p^2 \rangle^{1/2}$ , and  $\langle r_n^2 \rangle^{1/2}$  respectively.  $\langle r_{n,\sigma}^2 \rangle^{1/2}$  denotes the RMS radius of the last valence neutron. Experimental values are adopted from Ref. [41]. All units are in fm.

	$\langle r_m^2 \rangle^{1/2}$	$\langle r_p^2 \rangle^{1/2}$	$\langle r_n^2 \rangle^{1/2}$	$\langle r_{n,\sigma}^2 \rangle^{1/2}$
THSR	3.73	2.42	4.25	8.94
Exp [41]	2.91	2.36	3.09	7.98

The density distribution is shown in Fig. 5 to illustrate the structure of the  $1/2^+$  ground state and the giant extension of the last valence neutron. To obtain the density distribution, we first rewrite the intrinsic wave function  $|\Psi\rangle$  of  $^{11}\text{Be}$  as

$$|\Psi\rangle = C\mathcal{A}[\Phi^{\text{THSR}}(^{10}\text{Be})\phi_{11}(\mathbf{r}_{11})], \quad (11)$$

where  $\mathcal{A}$  is the antisymmetrizer and  $C$  is a normalization constant. Then the density distribution  $\rho(\mathbf{r}')$  of the last valence neutrons is defined as

$$\rho(\mathbf{r}') = N_c \langle \Phi^{\text{THSR}}(^{10}\text{Be})\phi_{11}(\mathbf{r}_{11}) | \delta(\mathbf{r}_{11} - \mathbf{X}_G - \mathbf{r}') | \Psi \rangle, \quad (12)$$

where  $N_c$  is the normalization constant [37]. In Fig. 5, the sigma-orbit structure with a distribution falling into three different regions is observed in the  $y = 0$  cross section, which

is consistent with pioneer works. The blue ellipse nodal surface is clearly shown in this cross section. The last valence neutron is found to have a very large distribution up to 8 fm in both  $x$  and  $z$  directions, which explains the giant RMS radius obtained for this neutron. Comparing with pioneer works with AMD method, the distribution in the central region is smaller in our calculation. This comes from the larger central part of nucleon-nucleon interaction in Eq. 8, which leads to a stronger  $\alpha$ - $\alpha$  attraction and closer  $\alpha$ - $\alpha$  distance. The neutron distribution is thus reduced because of the Pauli blocking from two  $\alpha$ -clusters.

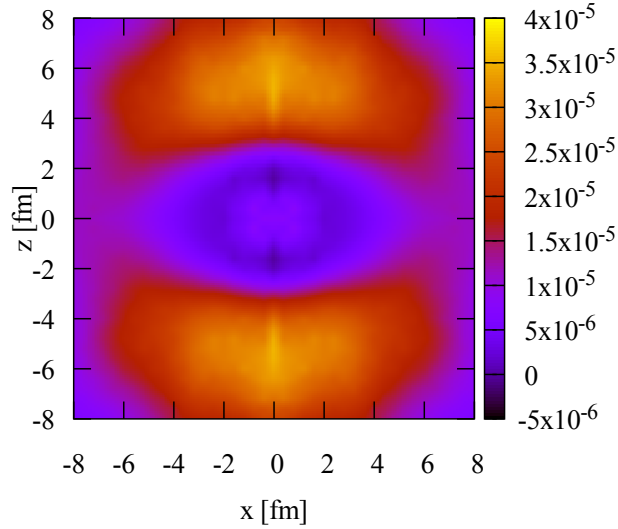


FIG. 5. Density distribution of valence neutrons occupying the  $\sigma$ -orbit in the intrinsic  $1/2^+$  state of  $^{11}\text{Be}$ . The color scale of each point in the figure is proportional to the nucleon density in the  $x - z$  plane of the  $y = 0$  cross section. The unit of the density is  $\text{fm}^{-3}$ .

We use the angular momentum projection technique to extract the spectroscopic factor  $S_{2s}$  from the ground state of  $^{11}\text{Be}$ . This is obtained by calculating the following squared overlap

$$\begin{aligned} S_{2s} &= N | \langle (\hat{P}_{0,0}^0 \Psi^{\text{THSR}}(^{10}\text{Be})) \phi_{11}(\mathbf{r}_{11}) | \hat{P}_{1/2,1/2}^{1/2} \Psi \rangle |^2 \\ &= 0.907. \end{aligned} \tag{13}$$

Here  $N$  is the coefficient originates from normalization and many body effects. Physically, this means that the probability amplitude of the  $|0^+ \otimes 2s_{1/2}\rangle$  occupation is about 91% for the  $1/2^+$  ground state of  $^{11}\text{Be}$ . This value is almost the same as the value 93% predicted

theoretically by Vinh Mau et al. in Ref. [40]. Our result is larger than the shell model predictions 74% and 55% in Refs. [14, 15]. This may partially due to the fact that our THSR wave function emphasizes the long tail structure for valence neutron while shell model methods usually deal with shrunk structure of nuclei. Recent experimental results for the  $S_{2s}$  are reported by Lima et al. in Ref. [42]. The experimental values vary largely from 46% to 87% with large error bars. Our result locates within error bars of four experimental results but larger than others.

We also study how our new coupling strength  $V_{ls}^*$  affects the spectroscopic factor  $S_{2s}$ . With a smaller  $V_{ls}=2000$  MeV, the corresponding spectroscopic factor is  $S'_{2s}=0.933$  for the  $1/2^+$  ground state of  $^{11}\text{Be}$ . With our new coupling strength  $V_{ls}^*=3200$  MeV, the spectroscopic factor is  $S_{2s}=0.907$ , which is 2.6% smaller. This shows that our new  $V_{ls}^*$  reduces the probability of the  $|0^+ \otimes 2s_{1/2}\rangle$  occupation and increases the probability for the  $|2^+ \otimes 1d_{5/2}\rangle$  occupation in the  $1/2^+$  ground state, which is also critical for the intruder ground state of  $^{11}\text{Be}$  [40].

In summary, we performed a self-consistent calculation for the exotic nucleus  $^{11}\text{Be}$  and other Be isotopes. The newly introduced valence neutron creator provides a correct description for the nodal surface for the  $\sigma$ -binding wave function in the ground state of  $^{11}\text{Be}$ . Ground state energies and single-neutron separation energies, which fit experimental results, are obtained for the  $^8\text{--}^{11}\text{Be}$  isotopes by systematic calculations with this new THSR wave function and isospin-dependent spin-orbit interaction strength. The low energy spectrum calculated has the right ordering but remains slightly diluted. Explicit consideration of low lying states in  $^{10}\text{Be}$  may be necessary to improve. However, the intruder ground state  $1/2^+$  with positive parity is correctly reproduced what is not easy to achieve. The neutron halo structure observed from experiments is illustrated with calculations of very large RMS radii and density distributions. The giant spatial distribution of the last valence neutron is also obtained, which agrees well with the phenomenological extraction from experimental data. We also calculate and discuss the effects of the spectroscopic factor  $S_{2s}$  for the  $1/2^+$  ground state of  $^{11}\text{Be}$ . This investigation opens up further evolution of the nonlocalized clustering approach to the  $\beta$ -unstable region and provides very satisfying insights for the exotic properties of the neutron rich nucleus  $^{11}\text{Be}$ .

## ACKNOWLEDGMENTS

This work is supported by the National Natural Science Foundation of China (grant nos 11535004, 11035001, 11375086, 11105079, 10735010, 10975072, 11175085 and 11235001), by the National Major State Basic Research and Development of China (grant no 2016YFE0129300), by the Research Fund of Doctoral Point (RFDP), grant no. 20100091110028, and by the Science and Technology Development Fund of Macao under grant no. 068/2011/A. The authors would like to thank Professor Yanlin Ye, Professor Massaki Kimura, Dr. Hantao Li for valuable discussions.

---

- [1] M. G. Mayer, Phys. Rev. **78**, 16 (1950).
- [2] S. S.-L. Zhang and G. Vignale, Phys. Rev. Lett. **116**, 136601 (2016).
- [3] A. Matos-Abiague and J. Fabian, Phys. Rev. Lett. **115**, 56602 (2015).
- [4] C. W. Groth, M. Wimmer, A. R. Akhmerov, J. Tworzydło, and C. W. J. Beenakker, Phys. Rev. Lett. **103**, 196805 (2009).
- [5] Z. Wang, X.-L. Qi, and S.-C. Zhang, Phys. Rev. Lett. **105**, 256803 (2010).
- [6] B. D. Cullity and C. D. Graham, Introduction to Magnetic Materials (John Wiley & Sons, 2011).
- [7] D. J. Griffiths, Introduction to Quantum Mechanics (Pearson Education India, 2005).
- [8] N. Itagaki, S. Okabe, and K. Ikeda, Phys. Rev. C **62**, 34301 (2000).
- [9] Y. Kanada-En'yo and H. Horiuchi, Phys. Rev. **666**, 24305 (2002).
- [10] J. Chen, J. L. Lou, Y. L. Ye et al., Phys. Rev. C **93**, 34623 (2016).
- [11] T. Aumann, A. Navin, D. P. Balamuth et al., Phys. Rev. Lett. **84**, 35 (2000).
- [12] J. Winfield, S. Fortier, W. Catford et al., Nucl. Phys. A **683**, 48 (2001).
- [13] N. Fukuda, T. Nakamura, N. Aoi et al., Phys. Rev. C **70**, 054606 (2004).
- [14] T. Otsuka, N. Fukunishi, and H. Sagawa, Phys. Rev. Lett. **70**, 1385 (1993).
- [15] B. A. Brown, Prog. Part. Nucl. Phys. **47**, 517 (2001).
- [16] H. Li and Z. Ren, Science China Phys., Mechanics & Astronomy **57**, 1005 (2014).
- [17] W. Y. So, K. S. Choi, M.-K. Cheoun, and K. S. Kim, Phys. Rev. C **93**, 54624 (2016).
- [18] Y. Funaki, H. Horiuchi, A. Tohsaki, P. Schuck, and G. Röpke, Prog. Theor. Phys. **108**, 297

- (2002).
- [19] M. Lyu, Z. Ren, B. Zhou, Y. Funaki, H. Horiuchi, G. Röpke, P. Schuck, A. Tohsaki, C. Xu, and T. Yamada, *Phys. Rev. C* **91**, 014313 (2015).
  - [20] M. Lyu, Z. Ren, B. Zhou, Y. Funaki, H. Horiuchi, G. Röpke, P. Schuck, A. Tohsaki, C. Xu, and T. Yamada, *Phys. Rev. C* **93**, 54308 (2016).
  - [21] A. Tohsaki, H. Horiuchi, P. Schuck, and G. Röpke, *Rev. Mod. Phys.* **89**, 11002 (2017).
  - [22] A. Tohsaki, H. Horiuchi, P. Schuck, and G. Röpke, *Phys. Rev. Lett.* **87**, 192501 (2001).
  - [23] B. Zhou, Z. Ren, C. Xu, Y. Funaki, T. Yamada, A. Tohsaki, H. Horiuchi, P. Schuck, and G. Röpke, *Phys. Rev. C* **86**, 014301 (2012).
  - [24] T. Yamada and P. Schuck, *Eur. Phys. J. A* **26**, 185 (2005).
  - [25] T. Suhara, Y. Funaki, B. Zhou, H. Horiuchi, and A. Tohsaki, *Phys. Rev. Lett.* **112**, 062501 (2014).
  - [26] B. Zhou, Y. Funaki, H. Horiuchi, Z. Ren, G. Röpke, P. Schuck, A. Tohsaki, C. Xu, and T. Yamada, *Phys. Rev. Lett.* **110**, 262501 (2013).
  - [27] B. Zhou, Y. Funaki, H. Horiuchi, Z. Ren, G. Röpke, P. Schuck, A. Tohsaki, C. Xu, and T. Yamada, *Phys. Rev. C* **89**, 034319 (2014).
  - [28] C. Xu and Z. Ren, *Phys. Rev. C* **73**, 041301 (2006).
  - [29] Y. Ren and Z. Ren, *Phys. Rev. C* **85**, 044608 (2012).
  - [30] W. He, Y. Ma et al., *Phys. Rev. Lett.* **113**, 032506 (2014).
  - [31] Z. Yang, Y. Ye et al., *Phys. Rev. Lett.* **112**, 162501 (2014).
  - [32] M. Spieker, S. Pascu, A. Zilges, and F. Iachello, *Phys. Rev. Lett.* **114**, 192504 (2015).
  - [33] V. Yu. Denisov, O. I. Davidovskaya, and I. Yu. Sedykh, *Phys. Rev. C* **92**, 014602 (2015).
  - [34] R. G. Lovas, R. J. Liotta, A. Insolia, K. Varga, and D. S. Delion, *Phys. Rep.* **294**, 265 (1998).
  - [35] I. J. Thompson and M. V. Zhukov, *Phys. Rev. C* **53**, 708 (1996).
  - [36] R. Álvarez-Rodríguez, A. S. Jensen, E. Garrido, and D. V. Fedorov, *Phys. Rev. C* **82**, 34001 (2010).
  - [37] H. Horiuchi, *Prog. Theor. Phys. Suppl.* **62**, 90 (1977).
  - [38] M. Wang, G. Audi, A. H. Wapstra, F. G. Kondev, M. MacCormick, X. Xu, and B. Pfeiffer, *Chinese Phys. C* **36**, 1603 (2012).
  - [39] J. H. Kelley, E. Kwan, J. E. Purcell, C. G. Sheu, and H. R. Weller, *Nucl. Phys. A* **880**, 88 (2012).

- [40] N. Vinh Mau, Nucl. Phys. A **592**, 33 (1995).
- [41] I. Tanihata, H. Savajols, and R. Kanungo, Prog. Part. Nucl. Phys. **68**, 215 (2013).
- [42] V. Lima, J. A. Scarpaci et al., Nucl. Phys. A **795**, 1 (2007).